Mass Balance

7

Michiel van den Broeke and Rianne Giesen

7.1 Introduction

In this chapter we discuss the methods used to assess temporal mass changes of different ice masses—valley glaciers, ice caps and ice sheets. We provide definitions of the key terminology in Sect. 7.2 and discuss the main methods to observe and model glacier mass balance in Sect. 7.3. Next, we present the specific application of these methods to valley glaciers and ice caps in Sect. 7.4 and to the two large ice sheets of Antarctica (Sect. 7.5) and Greenland (Sect. 7.6). The reason for this subdivision is that the ice sheets are large enough to allow for direct observation of mass changes by satellite remote sensing and *dynamical downscaling* of surface processes (using for example regional climate models), while valley glaciers and ice caps are usually so small that they require *statistical downscaling* of satellite observations or global/regional atmospheric model output.

7.2 Definitions

To be specific, let us consider an ice sheet or glacier which terminates in the ocean, so that it has a *grounding line* where it goes afloat. Glacier mass balance (MB, denoted as B, kg y^{-1}) represents the temporal change of glacier mass M_i, which, if we neglect basal melting of grounded ice and assume that the grounding line position is stationary, is governed by the difference between surface mass balance (SMB, denoted S) and ice discharge across the grounding line (D):

M. van den Broeke (✉) · R. Giesen
Utrecht University, Utrecht, The Netherlands
e-mail: m.r.vandenbroeke@uu.nl

A. Fowler and F. Ng (eds.), *Glaciers and Ice Sheets in the Climate System*, Springer Textbooks in Earth Sciences, Geography and Environment,
https://doi.org/10.1007/978-3-030-42584-5_7

$$\frac{\partial M_i}{\partial t} = S - D. \tag{7.1}$$

Equation (7.1) states that the mass balance of a glacier can be regarded as the sum of mass exchange processes at the ice-atmosphere interface (snowfall, sublimation, meltwater runoff) and at the ice-ocean interface (solid ice discharge, basal melt). With the grounded part of the ice sheet defined as the region of interest, the melt beneath floating glacier tongues and ice shelves, which is difficult to quantify (see Chaps. 4 and 5 on tidewater glaciers and ice shelf-ocean interactions), does not have to be included in the mass balance equation. However, when the grounding line migrates, the loss of the overlying ice must be taken into account. Ice discharge represents the flux of ice across the grounding line of the glacier or ice sheet, and is determined by the thickness and vertically averaged horizontal ice flow velocity component normal to the grounding line. Ice flow is the sum of deformation and basal sliding, as discussed in Chaps. 1 and 3. The surface mass balance S represents the sum of all mass fluxes towards and away from the glacier's snow/ice surface (the latter fluxes taken as having negative sign). It is given by

$$S = P + R - U_s - U_{ds} - E_{ds} - M, \tag{7.2}$$

where P is solid precipitation (snow, hail, freezing cloud droplets), R is rainfall, U_s and U_{ds} are sublimation from the surface and drifting snow particles, respectively, E_{ds} is erosion of snow by divergence of the drifting snow transport and M is meltwater runoff. The accumulation and ablation zones of a glacier are defined as the areas where $S > 0$ and $S < 0$, respectively. These zones are separated by the equilibrium line, where $S = 0$. Glaciers form at any land-based location where S is positive for numerous consecutive years; this time span must be large enough for glacier ice to form out of the slow compression and sintering of the lowest firn layers.

In the surface mass balance Eq. (7.2), runoff M is determined by the liquid water balance, which is the sum of all sources (water vapour condensation, rainfall and melt) and (negatively signed) sinks (refreezing and capillary retention) of liquid water:

$$M = R + C + M_s - R_s - F, \tag{7.3}$$

where C is condensation of water vapour due to the vertical turbulent exchange of atmospheric moisture, M_s is surface meltwater production, R_s is retention of liquid water in the snow/firn by capillary forces and F is refreezing. By including these subsurface processes ('internal accumulation'), S is formally referred to as the 'climatic mass balance' [1]. Instead of evaluating surface mass balance over the entire glacier surface, S is often measured locally as mass per unit time per unit area. This quantity is called the specific surface mass balance (abbreviated as SSMB), and we will denote its value as Σ; it has the same components as S but is expressed in kg m^{-2} y^{-1} or mm water-equivalent (mm w.e.) y^{-1}. These local or in situ measurements form the basis for spatial interpolation that in the end must yield the glacier surface mass balance.

7.3 Methods

In this section we describe the key methods used to determine the mass balance of valley glaciers, ice caps and ice sheets. We start with in situ SSMB observations in ablation and accumulation areas. A partial solution for the poor temporal and spatial coverage of SSMB observations (Sect. 7.3.1) over glaciers is provided by remote sensing techniques. To date, however, no technique exists that directly measures SSMB from space, and this gap is often filled by using atmospheric models. Recent developments in remote sensing and regional climate modelling now offer three other methods to estimate glacier mass balance indirectly, which are briefly discussed below (Sects. 7.3.2–7.3.4).

7.3.1 In Situ Observations

Because of the large variability in its components, SSMB can vary greatly from place to place and from year to year. As a result, it is necessary to perform numerous and repeated observations of SSMB (and of discharge D) in order to establish whether a glacier has positive or negative mass balance, i. e., whether it is growing or shrinking under present climate conditions. The simplest way to do this is to fix a stake into the ice/snow of the ablation/accumulation zone of a glacier and return to it one year later to measure how the surface level has changed (or to monitor the change continuously with electronic sensors; Fig. 7.1). Over a year, the length difference of the part of the stake that protrudes above the ice (Δh), multiplied by the density ρ of the ablated ice (≈ 910 kg m^{-3}) or the accumulated snow (to be measured), yields the value of Σ:

$$\Sigma = \rho \Delta h, \tag{7.4}$$

but several problems of logistical and scientific nature arise with this method. Glaciers and ice sheets are not easily accessible, making these measurements expensive. In mild and/or wet regions, annual ice ablation and snow accumulation of up to several metres pose serious problems for stake observations (the stakes need to be long, and their drill holes deep), while obtaining reliable snow density profiles over deep layers is cumbersome. It is often unclear how representative single-point measurements are for a larger area. Finally, the annual measurements must be performed at the same time each year. As a result, reliable in situ SSMB datasets measured on ice sheets and glaciers with long time span and high spatial resolution are scarce. In the accumulation zone of a glacier, other interpretation problems arise: here, stake measurements tell us nothing about refreezing and retention (internal accumulation) so that SSMB cannot be directly determined. To circumvent this problem, SSMB can also be obtained by drilling a firn core through multiple annual layers and subsequently measuring the amount of mass that has accumulated since a well-dated horizon (see Chap. 12 on ice cores); the horizon could be an acid layer deposited after a large volcanic eruption (Fig. 7.2) or a radioactive layer deposited after a nuclear test. In high-accumulation areas, seasonal cycles in inert chemical species

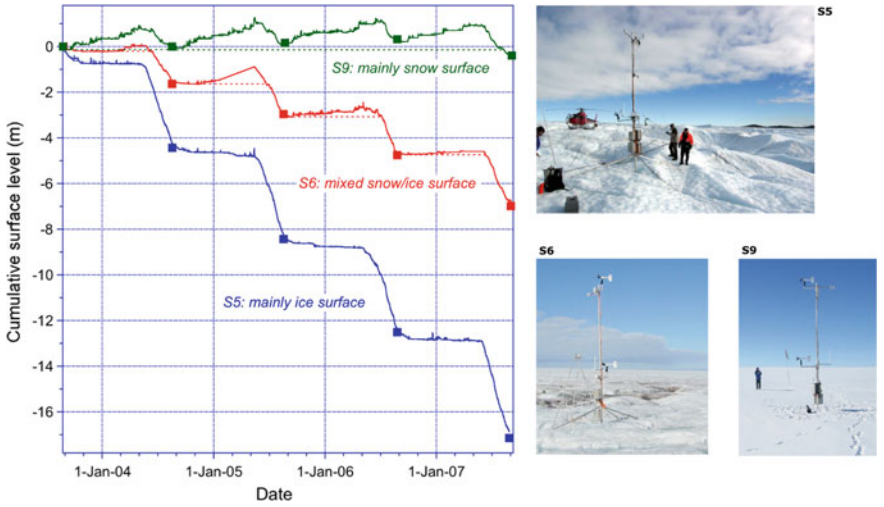

Fig. 7.1 Cumulative sonic height ranger observations along the K-transect, west Greenland, August 2003–August 2007. Site S5 is situated at ≈500 m a.s.l., S6 at ≈1000 m a.s.l. and S9 at ≈1500 m a.s.l., close to the equilibrium line. The build-up of a winter snow layer and its ablation in spring and summer is clearly visible in the middle ablation zone (S6). Snow accumulation and ablation approximately cancel near the equilibrium line (S9). At the lowest site (S5) all snow is blown in crevasses so that almost no winter snow accumulates. Images on the right show the measurement sites, including mass balance stakes and automatic weather stations (AWSs). The K-transect is a mass balance stake array of eight sites where annual SSMB and ice velocity have been measured since 1990

or physical characteristics of the snow and ice layers may be detected and counted to yield time series of SSMB. A powerful tool for locating reflection horizons in the firn so as to obtain high spatial resolution accumulation data is snow radar, which can be mounted on an airplane or towed behind a snowmobile to connect drilling sites. An overview of SSMB measurement techniques in polar (low) accumulation areas is provided by Eisen et al. [2].

Once sufficient reliable SSMB observations for a glacier are obtained, a map can be made using interpolation and extrapolation, thus yielding a value for glacier surface mass balance. When doing this one must carefully select the interpolation procedure and quantify the uncertainty in between the observations. As an example, the left panel of Fig. 7.3 shows an accumulation map of Dronning Maud Land, East Antarctica, based on the interpolation of sparse SSMB observations (black dots, [3]). The map predicts low accumulation in a region to the west of a transect near the coast (encircled), where automated equipment was subsequently installed. Upon return one year later, it appeared that SSMB was a factor 2.5 higher, and equipment had to be dug out (inset in Fig. 7.3). Even localized and unpronounced topographic features, in this case an ice rise, can apparently introduce significant local snowfall maxima that are not resolved by the sparse SSMB observations; these can nowadays be better identified using high resolution regional climate models (right panel in

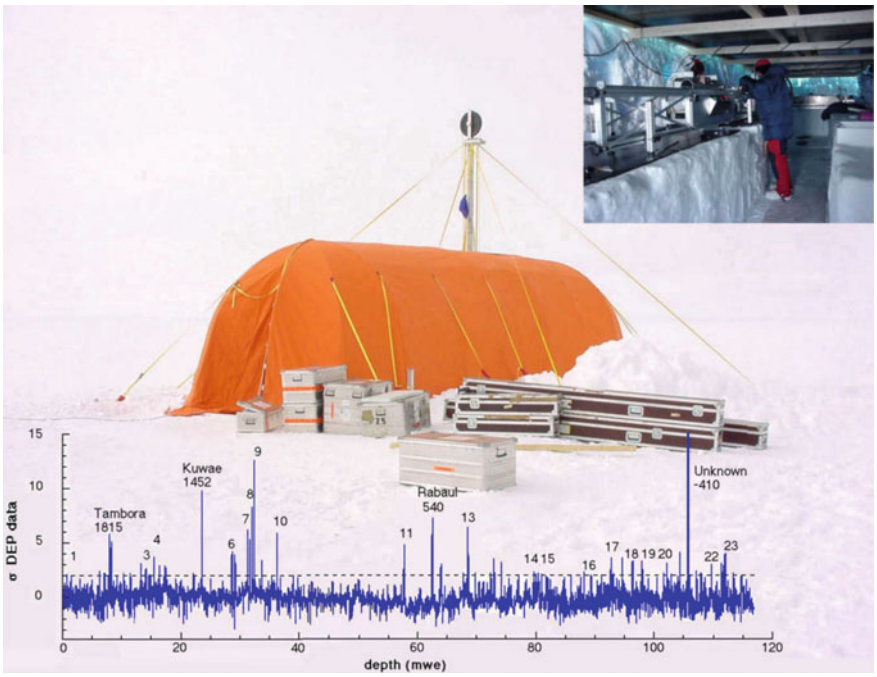

Fig. 7.2 Experimental setup for medium-deep ice core drilling, including on-site dating using a di-electrical profiling (DEP) instrument in a snow trench. The graph shows dated volcanic peaks as a function of depth (converted to metres of water equivalent, m w.e., using firn density)

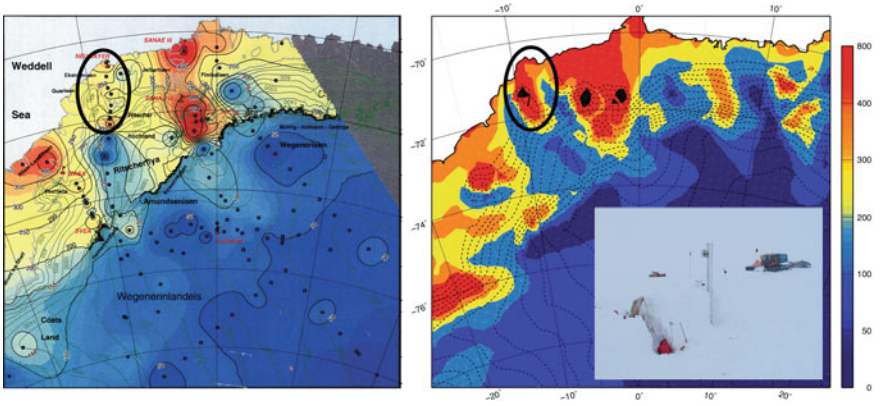

Fig. 7.3 SSMB map (kg m^{-2} y^{-1}) of Dronning Maud Land, East Antarctica, based on (left) the interpolation of observations (black dots) using kriging [3] and (right) calculations of a regional climate model at 27 km horizontal resolution [4]. Encircled is the area where automated equipment was installed that unexpectedly needed digging out after only a single year of operation (inset). Comparison of the two maps shows that numerous small-scale, topographically-forced accumulation features visible on the modelled map are absent from the interpolation-based map

Fig. 7.3). Comparison of the two panels in Fig. 7.3 shows more examples of such deficiency of interpolating sparse SSMB observations.

Even with sufficient coverage, in situ measurements of SSMB do not provide information about the magnitude of the various SSMB [Eq. (7.2)] or liquid water balance components [Eq. (7.3)]. For instance, a small yet positive SSMB value can result from any combination of accumulation and ablation processes, as long as the latter are smaller than the former. This poses a serious interpretation problem: without knowing the magnitude of individual SSMB components, it is difficult to relate mass balance changes to changes in climate. This can locally be remedied by installation of an automatic weather station (AWS) that is equipped with a sonic height ranger to detect individual accumulation and ablation events. Ideally, several AWSs are installed along a transect so as to obtain elevational gradients in SSMB components. Figure 7.1 shows examples of such time series from the ablation zone of the west Greenland Ice Sheet. If, apart from the standard variables of wind speed, temperature and humidity, an AWS also measures the surface radiation balance (incoming and outgoing shortwave and longwave radiation), then melt and sublimation fluxes can be explicitly quantified in combination with a surface energy balance model (see Chap. 6).

7.3.2 Satellite/Airborne Altimetry

Repeat satellite/airborne altimetry using radar/laser altimeters mounted on planes and various satellites (ERS1/2, ICESat, Envisat, CryoSat-2) yields changes in ice sheet volume, as further detailed in Sect. 13.4. The main instrument limitations arise from laser degradation and radar altimeters having an unknown penetration depth in snow, depending on (time-varying) firn density [6]. Before the launch of Cryosat-2 in 2010, radar altimeters did not resolve the narrow, fast flowing outlet glaciers, which are expected to react most rapidly to environmental changes. The laser altimeter onboard ICESat did capture these thinning glaciers in detail [7], but laser altimeters have limited spatial resolution and are sensitive to clouds, prohibiting the collection of continuous time series in high-accumulation (i.e., frequently overcast) areas. Moreover, degradation of the lasers in time requires temporally-varying corrections to be made.

The main methodological uncertainty in altimetry is that the vertical velocity at the ice sheet surface represents the sum of multiple processes, i.e., surface mass exchange (melt, sublimation, snowfall), compaction of the firn layer, and the downward movement of the firn/ice interface caused by divergence in the ice flow (Fig. 7.4, [8]); also see Sect. 13.4. A small basal melt term and vertical bedrock motion are usually neglected. To translate volume changes to mass changes therefore requires modelling of surface accumulation variability, which forces changes in firn mass and depth, and firn densification rate, which forces changes in firn depth. Both these processes dominate ice sheet elevation changes in areas away from rapid dynamic changes [5,6]. The inset in Fig. 7.4 explains the confounding effect of accumulation variability on elevation changes: decadal variability in accumulation that otherwise

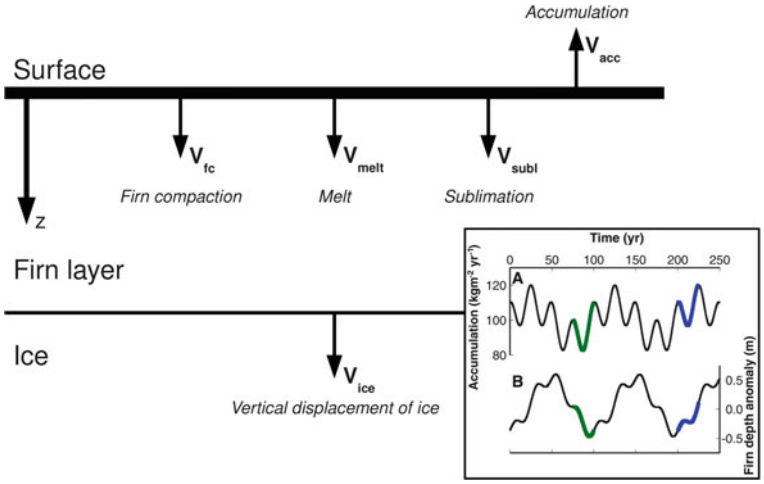

Fig. 7.4 Vertical velocity components that determine vertical displacement of the glacier surface. Inset shows artificial SSMB time series with 25 and 100 yr periodicity (upper curve) and the resulting surface elevation trends (lower curve) using a firn compaction model [5]. This figure is a combination of Figs. 11.11 and 11.13 of Chap. 11

has zero long-term trend (upper curve) results in slow firn depth changes (lower curve) that are easily misinterpreted as long term trends in ice sheet mass. Moreover, identically shaped decadal accumulation variations (indicated as green and blue in the upper curve) can result in the surface lowering or rising, depending on whether the anomaly takes place at average accumulation values that are below (green) or above (blue) the long-term average. More discussion of the firn densification processes underlying such response is given in Chap. 11 (see Sect. 11.3.1, in particular). When corrected for these confounding effects, altimetry can provide glacier mass loss rates, yet the data do not discriminate between the different processes responsible for the mass changes, i. e., S or D.

7.3.3 Satellite Gravimetry

Satellite gravimetry uses data of the Gravity Recovery And Climate Experiment (GRACE) twin satellites, launched in 2002, and follow-up missions. The first great accomplishment of GRACE was that it proved beyond a doubt that the large ice sheets have been losing mass during the first decade of the twenty-first century (Fig. 7.5). Like altimetry, GRACE does not discriminate between the various processes responsible for mass loss, but being independent of the other two methods and as the only method that measures mass change directly, GRACE provides valuable verification data for other techniques. Methodological uncertainties arise from the large footprint ($\approx$300 km) and associated "leakage effects", which make GRACE less useful for smaller ice caps and glaciers. A large uncertainty is introduced by the post-glacial rebound correction in Antarctica (see Chap. 15). As with most satellite products, the

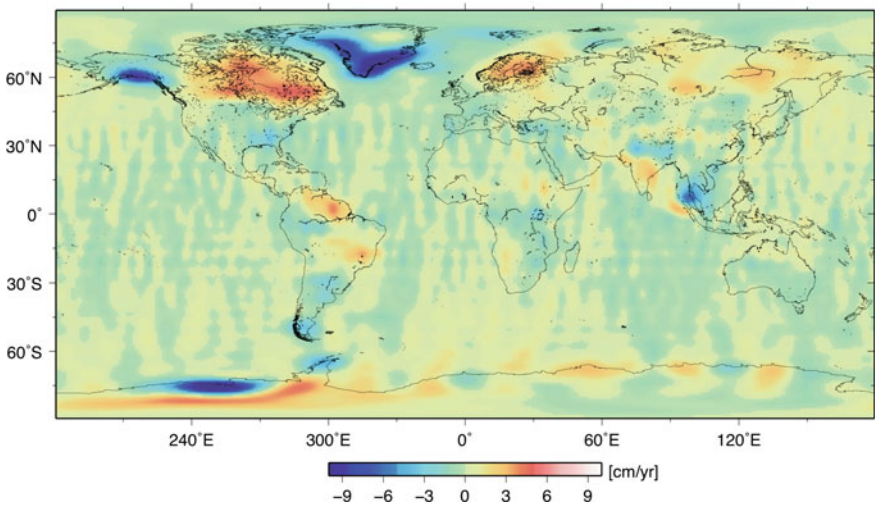

Fig. 7.5 Mass trend according to the Gravity Recovery And Climate Experiment satellite pair (GRACE, 2003–2010) in cm water equivalent per year. Figure courtesy of Bert Wouters (Utrecht University)

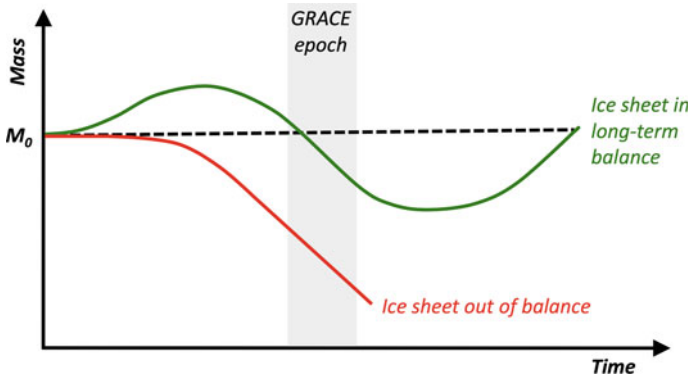

Fig. 7.6 Schematic drawing of glacier mass in time as measured by GRACE. Since GRACE does not measure the absolute mass of the glacier (M_0), and the time scale of operation is relatively short (about a decade), a mass loss observed by GRACE can be interpreted in multiple ways

relatively short observational period hampers a correct interpretation of the signal in terms of longer-term changes. Figure 7.6 illustrates this: in the absence of information about the total reference mass of the ice sheet (M_0), a negative mass trend in the brief GRACE time series could either indicate a slow mass oscillation of an ice sheet in long-term balance or declining mass of an ice sheet out of balance. Combining GRACE with other techniques can aid the interpretation of these signals (see later sections on mass balance of the Greenland and Antarctic Ice Sheets).

7.3.4 Mass Budget Method

The mass budget method quantifies the difference between surface mass gains (snowfall) and losses (meltwater runoff, sublimation), which together give the SMB (S, the red integration surface in Fig. 7.7) and lateral mass loss by solid ice discharge (D, the blue integration surface). The biggest disadvantage of the mass budget method is that it attempts to quantify the difference between three large terms (snow accumulation, solid ice discharge and meltwater runoff), each with relatively large uncertainties. As a result, the relative uncertainty in their difference can be substantial and sometimes even renders the sign of the glacier mass balance uncertain, i. e., it can not be stated with statistical certainty whether a glacier is losing or gaining mass. The major advantage of the mass budget method is that all individual mass balance components are quantified, providing valuable insights in the physical processes that drive ice sheet mass change [9].

An SMB value can be obtained through smart spatial interpolation of SSMB observations [10,11]; unfortunately, available SSMB data are often not sufficiently dense to arrive at robust estimates, and they provide limited insight in temporal variability. An alternative is offered by regional climate models, sometimes calibrated with SSMB observations [4,12–14]. Regional climate models explicitly resolve physical atmospheric processes leading to snowfall and melt, and run at higher resolution (typically 5–25 km) than global models (100–200 km). When evaluated against SSMB data, model errors are found to range between 5 and 30%, with the largest uncertainties occurring in regions of extreme (low or high) precipitation, or strong melting, or pronounced topography that is not well resolved by the model.

Quantifying solid ice discharge D requires observations of ice velocity and thickness at the grounding line. For this, feature tracking with interferometric synthetic aperture radar (InSAR) is used, which yields surface ice velocity with high accuracy

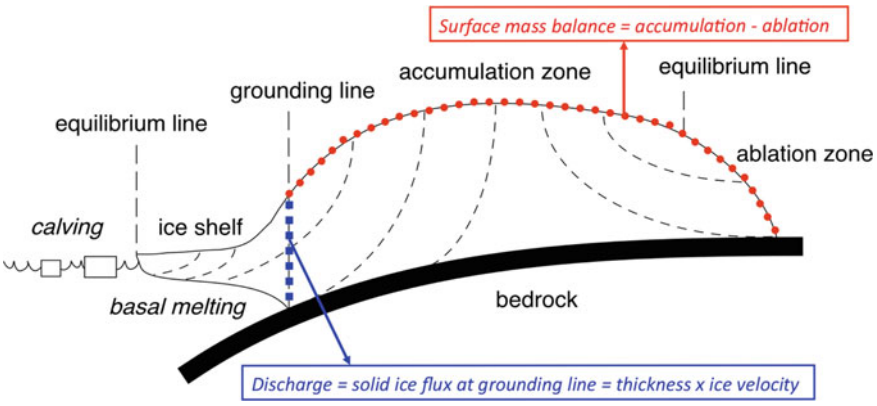

Fig. 7.7 Schematic cross-section of a marine- (left) and land-terminating (right) ice sheet. Dashed lines approximate ice flow lines. Symbols represent integration surfaces for the mass budget method: red symbols for surface mass balance (SMB) and blue symbols for solid ice discharge (D)

($< 5\%$ [9,15]). The principles of feature tracking are further explained in Sect. 13.3.3. The thickness of many ice streams has now been directly measured using airborne radar with sufficient accuracy (≈ 10 m). In regions where such data do not yet exist, satellite altimetry is used [16]; this, in combination with a flotation criterion, yields thickness with uncertainties of ≈ 100 m [17]. To convert elevation to thickness, a correction must be applied for the density of the firn mantle that covers the ice, e. g., using a steady-state firn compaction model [8]. For the Greenland Ice Sheet, where glacier tongues experience significant ablation in summer, this correction is less important. Finally, corrections must be made for glacier thinning and the mass flux associated with grounding line migration [9].

7.4 Valley Glaciers and Ice Caps

In this section we describe the application of the methods to assess the mass balance of valley glaciers and ice caps (GIC), which comprise all glaciers outside the ice sheets of Greenland and Antarctica.

7.4.1 In Situ Observations

GIC SSMB stake observations have been conducted since the late nineteenth century [18]. The earlier quantitative measurements were often made at single locations on a valley glacier and not repeated annually, hence they could not be used to determine the glacier's SMB. The longest continuous SMB record with glacier-averaged annual values dates back to 1946, when a measurement program was started on Storglaciären in northern Sweden. Since then, surface mass balance observations have been carried out on GIC in many regions of the world. The number of mass balance records is heavily biased toward the European Alps, Scandinavia and North America, where glaciers are relatively accessible. A sample of long cumulative SMB records for different regions is shown in Fig. 7.8. The three maritime valley glaciers in Norway had a net surface mass gain over the period 1960–2010, which is mainly a result of a few years with very high winter precipitation around 1990. All other glaciers in Fig. 7.8 show a net surface mass loss between 1960 and 2010, which often accelerated after the year 2000. Different GIC in the same region generally show similar interannual variability, although the absolute values of the SMB vary. Interannual variations in SMB are largest for the maritime glaciers in Norway with large amounts of solid precipitation, and smallest for the dry Arctic glaciers. These long SMB records are very valuable for the purpose of obtaining a first indication of mass changes in different regions. However, variations of the total cumulative change for the GIC within a region can be large and can thus complicate the upscaling of the measurements to estimate the mass change for the whole region.

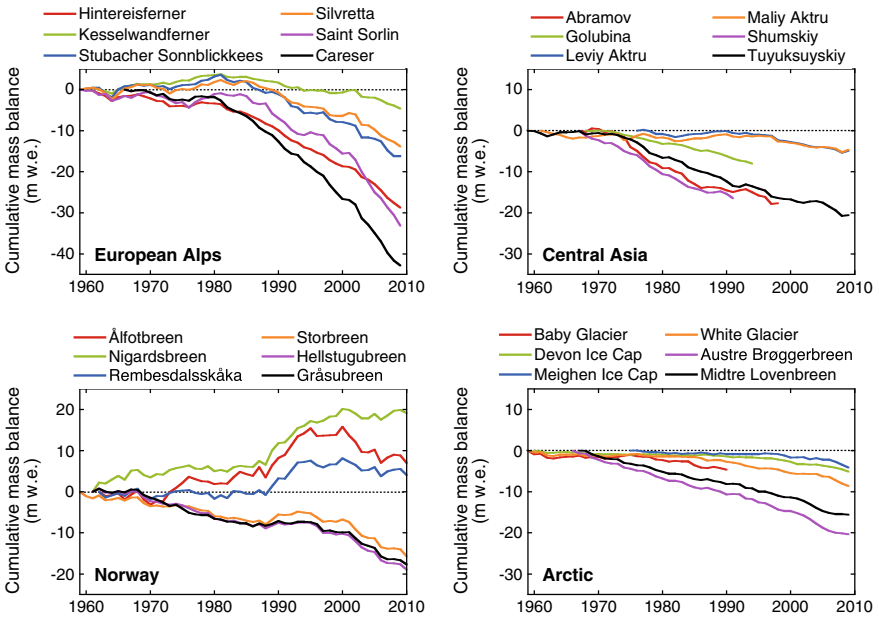

Fig. 7.8 Cumulative surface mass balance from measurements on glaciers in four regions of the world. Data provided by the World Glacier Monitoring Service (updated, and earlier issues, [19])

7.4.2 Modelling

While SSMB observations provide a wealth of information on the relation between climate and GIC mass changes, they are often supplemented by SMB models, in order to: (1) extend the period with mass balance measurements further back in time or into the future; (2) estimate SMB for glaciers without observations; (3) study the importance of different terms in the surface mass and energy balance; and (4) determine the sensitivity of the SMB to changes in climatic variables. Models of various degrees of complexity are used to compute GIC mass balance. The choice of model is usually determined by the available meteorological input data and observations for model calibration. Since positive mass contributions primarily come from solid precipitation, accumulation is generally simply derived from precipitation input data. A threshold temperature or temperature range is used to distinguish between rain and snow. On GIC outside the tropics, runoff from melting is the most important negative term in the surface mass balance. The following paragraphs discuss three models of different complexity (positive-degree-day, simple surface energy balance, full surface energy balance) that are commonly used to calculate surface melt.

The most simple model is the temperature-index or positive-degree-day (PDD) model, where ablation is assumed to be an empirical function of the sum of days with positive air temperatures (for a review of the method, see [20]). The melt rate changes considerably when the surface cover changes from snow to ice, as this affects the albedo; this is not reflected in the measured air temperature. It is therefore common

practice to use two different PDD melt factors: one for snow and one for ice. The values of these melt factors depend on the importance of the temperature-dependent fluxes (mainly longwave radiation and the turbulent fluxes) in the energy balance and need to be calibrated with ablation measurements from the glacier of interest. Since the PDD method implicitly assumes that seasonal variations in net solar radiation (which do not depend on air temperature) coincide with air temperature variations, this model only works when this is actually the case. Furthermore, since net solar radiation is combined with the temperature-dependent fluxes, the sensitivity of the melt rate to changes in air temperature is not correct. An often-used motivation for using a PDD model instead of a more sophisticated representation of the surface energy fluxes is that meteorological input data other than precipitation and air temperature are not available. However, a separation of the contributions by net solar radiation and the temperature-dependent fluxes can be made without requiring additional meteorological input data [21]. For a physical representation of the surface energy balance, it is important that the terms for net solar radiation and the temperature-dependent fluxes are added, not multiplied, as is done in some models.

Seasonal cycles of the SSMB components modelled with a PDD model and a simple surface energy balance (SEB) model are shown in Fig. 7.9 for two automatic weather station (AWS) sites on glaciers in Switzerland and Iceland. For the Swiss glacier, the seasonal cycles in net solar radiation and air temperature are rather similar and the SSMB calculated with the PDD model reproduces the measurements reasonably well. Compared to the surface energy fluxes modelled with the simple SEB model, the PDD model underestimates melt in spring and overestimates melt in

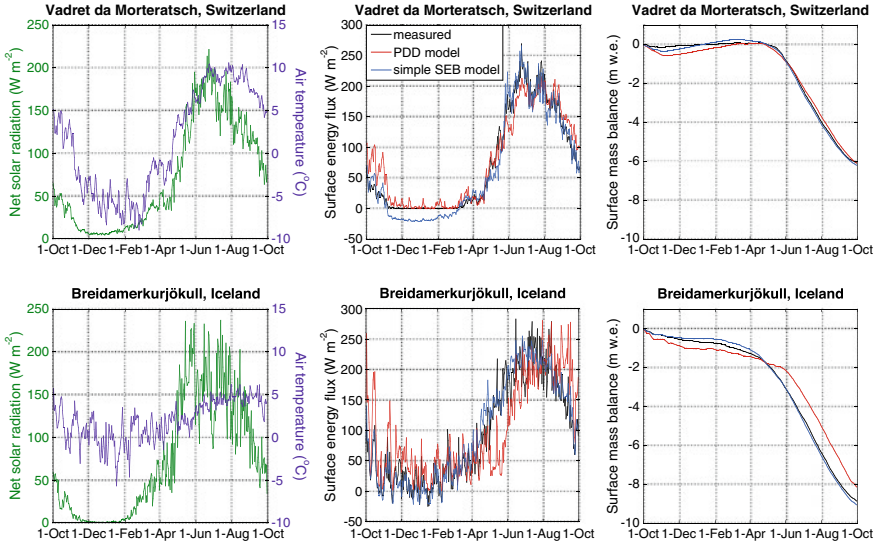

Fig. 7.9 Measured and modelled seasonal cycles of the surface energy flux and surface mass balance for AWS sites on Vadret da Morteratsch in Switzerland and Breiðamerkurjökull in Iceland. Results are obtained with a positive-degree-day (PDD) and a simple surface energy balance (SEB) model. Also shown are the measured seasonal cycles of net solar radiation and air temperature

the late summer and autumn. On the maritime Icelandic glacier, the seasonal cycle in air temperature has a low amplitude, while net solar radiation varies strongly through the year. Because the maximum in net solar radiation occurs well before the maximum air temperature, the PDD model considerably underestimates melt in spring, while there is too much melt from the late summer into the winter. Furthermore, the low-amplitude seasonal cycle in air temperature results in large melt factors and too large interdaily variations in the surface energy flux.

When meteorological variables like cloud cover, relative humidity and wind speed are also available, all fluxes in the surface energy balance can be calculated separately. This results in more realistic variations in the melt rate and allows for a thorough SMB sensitivity analysis to changes in meteorological variables. Input data can be either observations from weather stations situated on or near the glacier, or the output fields of high-resolution regional climate models. Since the observations at the weather stations or model gridpoints generally do not cover the full glacier altitudinal range, the input data are extrapolated over the glacier surface using simple functions of the variation of the meteorological variables with elevation. The surface energy fluxes are parameterized as functions of the meteorological input variables; many different parameterizations are available from the literature [22–24]. If available, measured surface energy fluxes are used to calibrate the model parameters. Most of these sophisticated SMB models include a layered subsurface model, which is used to treat the subsurface heat flux, routing of meltwater through the snowpack, and refreezing of meltwater in cold layers.

Figure 7.10 shows the SSMB map for the ice cap Hardangerjøkulen in southern Norway, calculated with a distributed SSMB model using input data from nearby weather stations. The annual SSMB is primarily a function of altitude, with the most positive values around the summit. Like many ice caps, Hardangerjøkulen has a relatively large and flat accumulation area (where $\Sigma > 0$), while most of the melt and runoff occurs on the steeper outlet glaciers. Deviations from the altitudinal mean

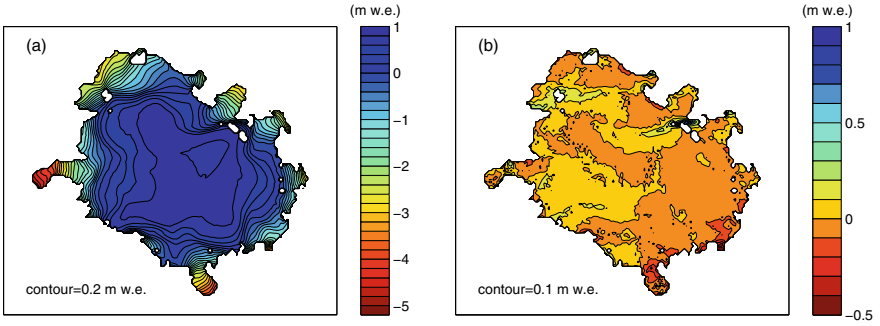

Fig. 7.10 **a** Annual mean and **b** altitudinal deviation of the SMB distribution of Hardangerjøkulen for the period 1961 to 1990, modelled with meteorological data. For each grid cell, the altitudinal deviation gives the local mass balance deviation from the mean surface mass balance for the corresponding 5 m altitude interval. Figure from [25]

mass balance, mainly resulting from differences in incoming solar radiation due to the orientation of the surface and shading by the surrounding topography, are considerable on some of the outlet glaciers.

7.4.3 Dynamical Response

All glaciers are slowly but continuously changing their geometry to respond to mass balance variations induced by changes in the climate. Especially after multi-year periods with a net positive or negative mass balance, the glacier area and surface elevation may change substantially. Since the SSMB at each position depends on its elevation, changes in the glacier geometry need to be taken into account both for interpreting mass-balance measurements and for modelling mass balance. Glacier maps are often updated after one to three decades, and reported surface mass balance values refer to the last available (most recent) glacier map for that year. This change of reference surface needs to be taken into account when comparing measured and modelled SSMB. Since the SSMB values encapsulate both geometric and climatic variations, changes in the mass balance cannot directly be related to climate forcing. For this purpose, the use of one constant reference surface is recommended.

Consecutive glacier maps provide an independent validation of in situ SSMB measurements. The surface elevation difference between two successive maps is multiplied by a representative density (usually ice density is taken) to obtain the total mass change. Differences between this geodetic mass balance and the cumulative annual SSMB measurements over the same period can be large, for example due to assumptions made in the extrapolation of stake measurements or the density used to calculate the geodetic mass balance [26].

In SSMB modelling, the available glacier maps can be used to account for changes in the glacier geometry. When such maps are not available, for example when modelling into the future, the SSMB model can be coupled to a dynamical ice model. A major advantage of such a coupled model is that changes in SSMB and glacier geometry are consistent. A drawback could be that the glacier geometry becomes unrealistic when the ice dynamics are not well represented. A simulation with a coupled model for Hardangerjøkulen in southern Norway illustrates the geometry response to changes in surface mass balance in a warming climate (Fig. 7.11). While the SSMB becomes more negative at all altitudes, the ice cap surface elevation lowers and the ice disappears from the highest ridges in the topography. As a result, there is no accumulation area left and the ice cap is bound to disappear completely.

7.4.4 Remote Sensing

In recent years, traditional stake measurements on GIC are being supplemented by remote sensing techniques like satellite/airborne altimetry and gravimetry (Sect. 7.3). Satellites are well suited to monitor large glaciers and ice caps in remote locations, nicely complementing the traditional measurement programs. Altimetry studies have

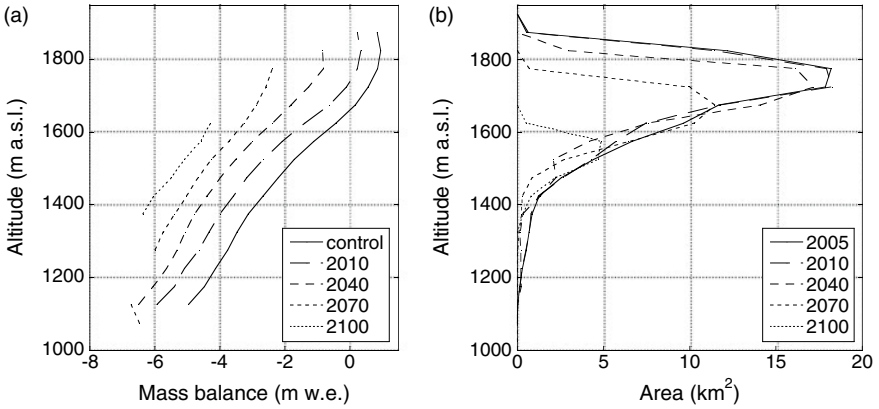

Fig. 7.11 Modelled **a** SMB profile and **b** area distribution for Hardangerjøkulen in 2010, 2040, 2070 and 2100, for a future climate projection with a temperature increase of 3 °C and precipitation increase of 10% between 1961–1990 and 2071–2000. The mass balance profile for the control climate (1961–1990) and the area distribution at the beginning of the simulation (2005) are also shown. Figure from [25]

revealed large mass losses on glaciers and ice caps in the Arctic regions [27,28] and Patagonia [29]. Attempts to derive mass changes in glaciated regions from GRACE have also been made [30], but the resulting estimates have large uncertainties introduced by the required GRACE corrections for other processes such as hydrology and seasonal snow.

7.5 Antarctic Ice Sheet

In the following sections we discuss the spatial and temporal variability of the mass balance of the Antarctic Ice Sheet (AIS). Here we may rely on insights from the mass budget method, which, as explained in Sect. 7.3, resolves the separate contributions made by the surface mass balance (SMB) and solid ice discharge (D).

7.5.1 Spatial SSMB Variability

Figure 7.12 shows on the left a map of SSMB based on output of the Regional Atmospheric Climate Model (RACMO2) for Antarctica at 27 km horizontal resolution [4]. This field represents the average for a 21-year period (1989-2009), obtained by forcing RACMO2 at the boundaries by data of the European Centre for Medium-range Weather Forecasts (ECMWF) interim re-analysis (ERA-Interim). The map correlates well with in situ SSMB observations from firn cores, stakes and snow pits (r = 0.87 for the AIS) and is therefore deemed reliable for a quantitative discussion.

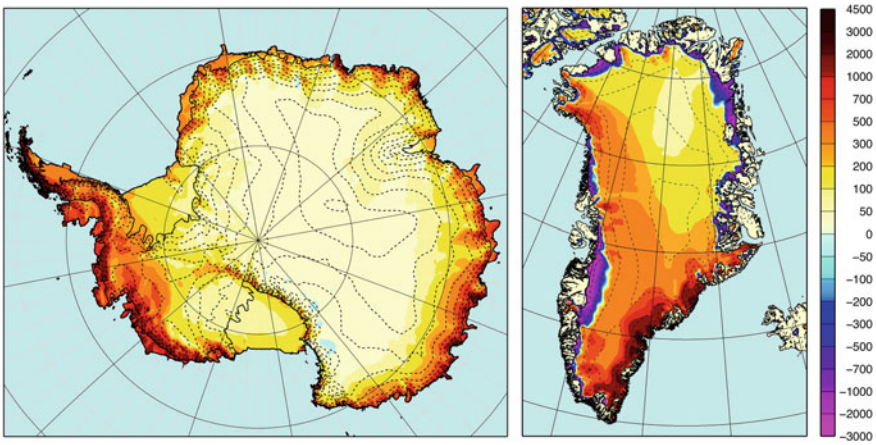

Fig. 7.12 Specific surface mass balance maps (kg m^{-2} y^{-1}) for the Antarctic Ice Sheet (left, [4]) and the Greenland Ice Sheet (right, [13]), based on a regional atmospheric climate model

As described in the preceding chapter, the large-scale flow around Antarctica is westerly north of the circumpolar pressure trough and easterly south of it. The only part of Antarctica that is exposed to the westerly circulation at lower latitudes is the Antarctic Peninsula (AP), which acts as a topographic barrier to the flow (similar to the Andes further north). Figure 7.12 shows that the orographic lifting of the relatively mild and humid air masses results in extreme precipitation rates in the western Antarctic Peninsula (> 4500 kg m^{-2} y^{-1}). For a typical near-surface snow density of 350 kg m^{-3}, this represents an annual snow layer depth of > 10 m; field parties operating at the spine of the Antarctic Peninsula confirm accumulation rates as high as one metre of snow per month. Further south, the circumpolar pressure trough includes three well-defined climatological low pressure areas that introduce a three-wave asymmetry in the zonal flow (see Sect. 6.4 and Fig. 6.6), regionally forcing persistent onshore atmospheric flow. This again results in orographic lifting and high precipitation rates in these areas, especially in coastal West Antarctica (> 1000 kg m^{-2} y^{-1}).

As a result of descending air motion, relatively dry areas are found at the lee side of topographic barriers, e. g., the eastern side of the Antarctic Peninsula receives less than 300 kg m^{-2} y^{-1}, an order of magnitude less than regions just 200 km to the west. Another example is Law Dome in coastal Wilkes Land, East Antarctica, which receives > 1500 kg m^{-2} y^{-1} at the eastern (upstream) side, and < 200 kg m^{-2} y^{-1} at the western (downstream) side. Evidence of pronounced orographic effects on the precipitation distribution can be found everywhere along the Antarctic coast, as previously discussed and shown in Fig. 7.3. Moist air seldom reaches the interior of the East Antarctic Ice Sheet; this region receives < 50 kg m^{-2} y^{-1} of snow and may justifiably be called a polar desert.

7.5.2 Blue Ice Areas

The Antarctic climate is too cold to allow for significant meltwater runoff; nearly all meltwater that is formed at the surface refreezes in the cold firn mantle. Only around 1% of the surface of the AIS represents ablation area; in these areas, the removal of mass is not driven by melting but by surface and drifting snow sublimation. When these processes persistently exceed snowfall, $\Sigma < 0$ and the 50–120 m thick firn layer may be completely removed, after which blueish glacier ice is exposed at the surface. This is why these areas are often referred to as blue ice areas (BIAs). The formation of BIAs requires two conditions to be met: (1) $\Sigma < 0$, i. e., the combined effect of drifting snow erosion and (drifting snow) sublimation should exceed snowfall; and (2) the firn layer must be exposed to the negative SSMB for a sufficiently long period that the entire firn layer can be removed. Since low ice velocity favours such long exposure, BIAs are often found in regions where nunataks (mountains that protrude through the ice and slow down the ice flow) are abundant, e. g., the Queen Fabiola Mountains in Dronning Maud Land and Allan Hills in Victoria Land.

We can define a minimum trajectory length L_{min} of ice flow through a region of negative SSMB, which is necessary to form blue ice:

$$L_{\text{min}} = \frac{m_{\text{firn}} V_{\text{ice}}}{|\Sigma|}, \tag{7.5}$$

where m_{firn} is the mass of the firn layer (kg m^{-2}) upstream of the ablation area, which can be calculated using a firn model (e. g., [8]), V_{ice} is the average surface ice velocity (m y^{-1}) and Σ (kg m^{-2} y^{-1}) is the average value of SSMB along the trajectory. In areas of fast ice flow, Eq. (7.5) implies that BIAs can develop only if $\Sigma < 0$ is highly negative, i. e., (snowdrift) sublimation and erosion are well developed. Byrd Glacier, which flows through the Transantarctic Mountains at relatively high velocity (Fig. 7.13) has blue ice over large parts of its surface. Recent advances in regional SSMB modelling over the AIS at high (≈ 5 km) horizontal resolution (Fig. 7.13a) predicts an extensive area in which $\Sigma < 0$ over the Byrd Glacier trunk [31]. Figure 7.13b shows that snowfall increases following the centre flowline towards sea level, but that ablating processes associated with drifting snow make SSMB negative over a ≈ 100 km stretch. If we substitute typical values for m_{firn} (20,000 kg m^{-2}), V_{ice} (800 m y^{-1}) and Σ (-200 kg m^{-2} y^{-1}) in Eq. (7.5), we find $L_{\text{min}} = 80$ km, which is smaller than the observed length of the ablation trajectory, indicating that the conditions for BIA development are met. Once formed, BIAs tend to persist, owing to their dark and smooth surface, which enhances summer sublimation and prevents fresh snow from attaching.

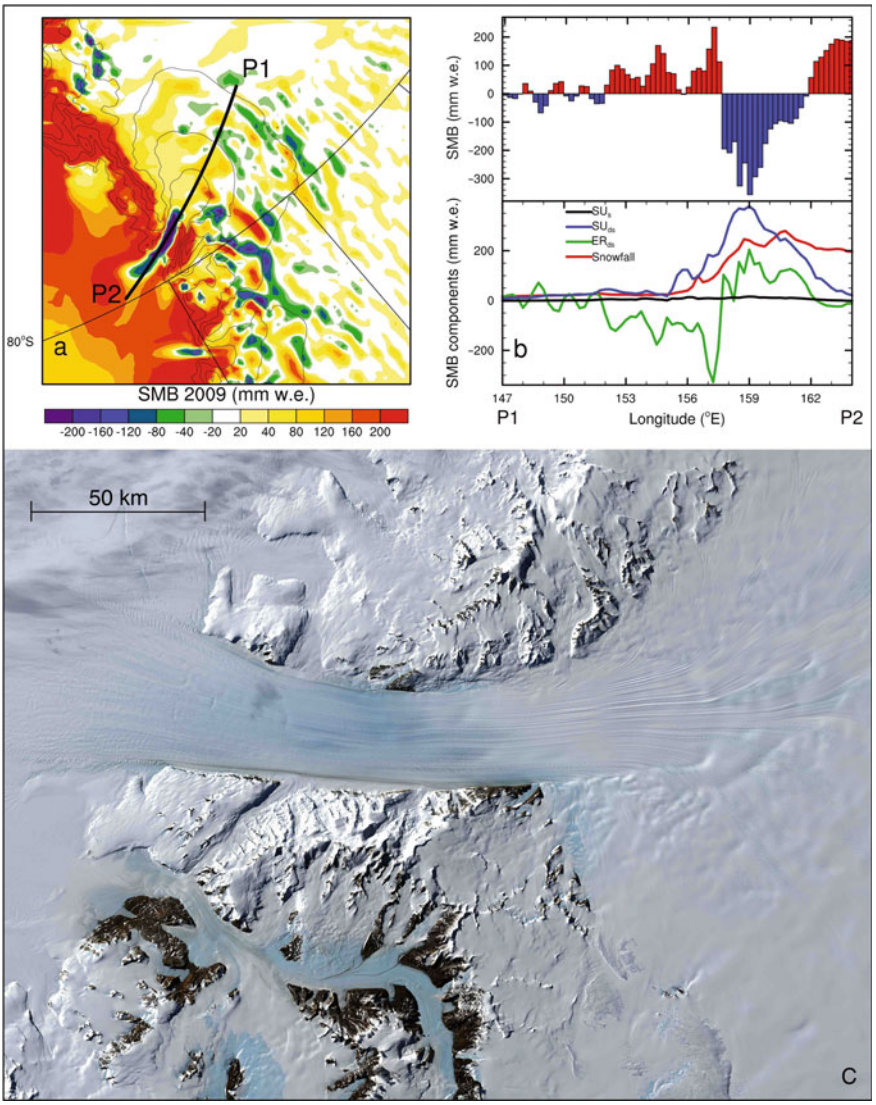

Fig. 7.13 **a** Specific surface mass balance map for the region of Byrd Glacier, based on a regional atmospheric climate model [31]; **b** SSMB components along flowline P1–P2; **c** MODIS image of Byrd Glacier

7.5.3 Temporal SSMB Variability

Improved estimates of SMB from regional climate modelling and D from remote sensing enable us to apply the mass budget method to the AIS for individual years

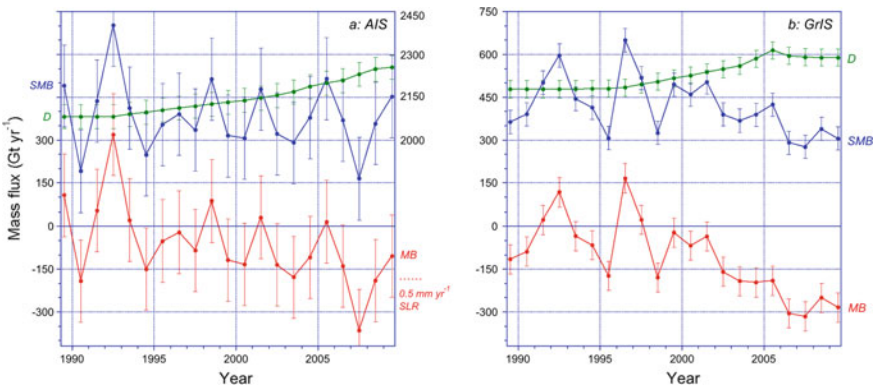

Fig. 7.14 Time series of surface mass balance (SMB, blue), solid ice discharge (D, green) and resulting ice sheet mass balance (B, red) for **a** the Antarctic Ice Sheet (AIS) and **b** the Greenland Ice Sheet (GrIS) in Gt y^{-1} [32]

in the period 1990–present. Before 1980, meteorological reanalysis products are unreliable in the Southern Hemisphere, while discharge observations are available since about 1990 [9]. Figure 7.14a shows the resulting time series of SMB (S), D and MB (B) for the grounded part of the Antarctic Ice Sheet. SMB does not show a significant trend. A notable feature in Fig. 7.14a is the large interannual variability in SMB, with year-to-year changes as large as 300 Gt y^{-1} (which is equivalent to a global sea level change rate of 0.8 mm y^{-1}). The standard deviation of ≈ 120 Gt y^{-1} represents just 6% of the 1989–2009 average SMB over the grounded part of the ice sheet (≈ 2100 Gt y^{-1}); this demonstrates that, even though the relative interannual variability of SMB is small, the variability in terms of absolute mass balance is very significant for the AIS, and it obscures trends in the total mass balance.

The increase in solid ice discharge D from the AIS is mainly caused by the acceleration of glaciers in coastal West Antarctica, which continues today, and by the acceleration of glaciers in the Antarctic Peninsula, mainly prior to 2005. Figure 7.15 shows that, compared to 1992, discharge from the AIS has increased by ≈ 170 Gt y^{-1} or 8% in 2009; as a result, MB has been persistently negative since 1994, except for three years with high snowfall (1998, 2001, 2005). Consequently, the AIS has contributed about 4 ± 2 mm to sea level rise between 1990 and 2010, which is about 7% of the total for that period [33].

7.6 Greenland Ice Sheet

In these final sections, we discuss the spatial and temporal variability of the mass balance of the Greenland Ice Sheet (GrIS). Its main difference when compared with the Antarctic Ice Sheet is the existence of a significant ablation area ($\Sigma < 0$), where meltwater runoff exceeds accumulation by precipitation. Although the GrIS is 8.5 times smaller than the AIS in volume, recent mass losses of the GrIS have exceeded that of the AIS.

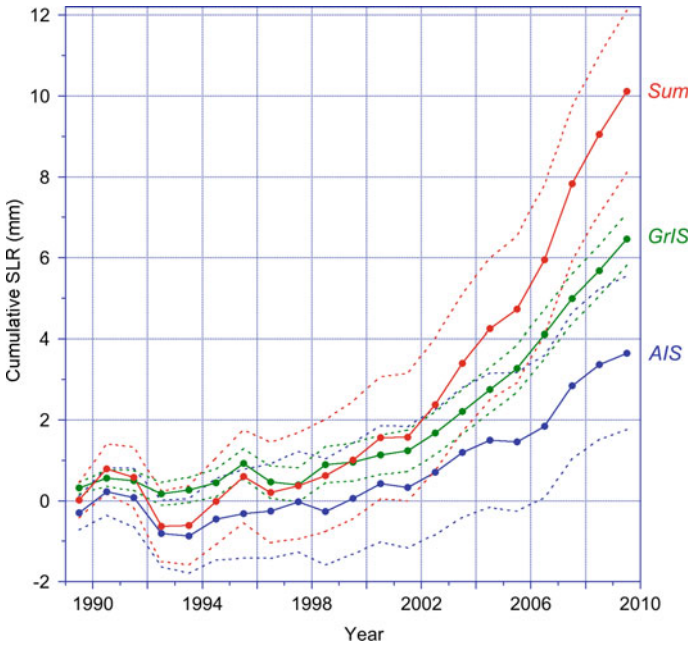

Fig. 7.15 Cumulative contribution to global sea level rise (SLR) from the Antarctic Ice Sheet (AIS, blue line) and the Greenland Ice Sheet (GrIS, green line) and their sum (red), in mm sea level equivalent. Dashed lines indicate uncertainty margins [32]

7.6.1 Spatial SSMB Variability

Figure 7.12 shows on the right a map of SSMB for the GrIS based on output of the Regional Atmospheric Climate Model (RACMO2) for Greenland at 11 km resolution [13]. The result correlates well with in situ SSMB observations from firn cores, stakes and snow pits (r = 0.95 for the GrIS). The most notable feature in Fig. 7.12 is the asymmetry: zones with high accumulation are found in the northwest and especially in the southeast of the ice sheet, where values in excess of 4000 kg m^{-2} y^{-1} (>10 m of snow) are predicted. These high snowfall rates are caused by the occasional northward migration of low-pressure areas through Davis Strait (west of the ice sheet) and the presence of the Icelandic Low, a semi-permanent low pressure system east of the southern tip of Greenland, respectively. These systems force relatively warm and moist air masses onto the steep ice sheet, creating orographic precipitation maxima similar to those found in Antarctica. Because of difficult access and the harsh climate conditions, there is a lack of direct SSMB observations from these regions so that large uncertainties remain. The high accumulation creates a steep ice sheet margin, preventing the formation of a wide ablation zone.

In contrast, the southwest and northeast of Greenland receive less than 200 kg m^{-2} y^{-1} of snowfall, the driest parts of the ice sheet in the northeast even less than 100 kg m^{-2} y^{-1}. In these regions, cloud cover is on average low, summer snowfalls are rare and solar irradiation high. As a result, the winter snow layer quickly melts

away in spring, exposing the dark glacier ice early in the melting season, followed by pronounced summertime melt and runoff. As a result, these parts of the GrIS have well-defined and relatively wide marginal ablation zones (purple colours in Fig. 7.12, $\Sigma < 0$). In the southwest, the ablation zone is 100–150 km wide and the lowest parts of the ice sheet experience annual ablation rates of up to 3500 kg m^{-2} y^{-1}. A notable feature in some of these marginal regions is the apparent absence of winter accumulation, and this is ascribed to the collection of snow in crevasses (see description in Fig. 7.1).

7.6.2 Temporal SSMB Variability

For the GrIS, reliable SMB time series can be reconstructed as far back as 1958, owing to better observational coverage in the northern hemisphere and hence more reliable atmospheric re-analysis products to drive regional climate models over the ice sheet. However, reliable estimates of D are only available since the early 1990s. Both SMB and D time series are displayed in Fig. 7.14b for the period 1989–2009; this compilation assumes constant discharge before 1992 and uses a linear interpolation to estimate D between those years with observations.

Unlike in Antarctica, where runoff is negligible, runoff variability strongly impacts interannual SMB variability on the GrIS. Years of low accumulation tend to cause higher summer ablation due to the lower albedo of bare ice, and therefore year-to-year variations in SMB can be as large as 400 Gt y^{-1}. The average standard deviation is 100 Gt y^{-1}, 24% of the average SMB (417 Gt y^{-1}), which is four times larger than the relative variability for the AIS.

Another contrast to the AIS is that the SMB shows a significant negative trend since about 2000, following atmospheric warming and increased runoff since the early 1990s. In combination with an increase in D since about 1996, which is the result of glacier acceleration in southeast, west and northwest Greenland [34], this has resulted in a persistently negative MB since 1999. Note that the large interannual variability in the beginning of the time series is not sustained during the recent period of strong melt. Between 1990 and 2009, the GrIS has contributed 6 ± 1 mm to post-1990 sea level rise, approximately 10% of the total sea level rise over this period (Fig. 7.15).

7.6.3 Role of the Liquid Water Balance

As noted above, runoff [M in Eq. (7.3)] is an important component of the SMB of the GrIS and recent trends therein. Figure 7.16 shows cumulative anomalies (relative to the reference period 1961–1990, when the ice sheet mass balance was approximately zero) of the major components of the liquid water balance (LWB): melt (green line), runoff (orange line) and rainfall (light blue line). The increase in melt clearly dominates changes in the LWB and hence the SMB, with an estimated 3000 Gt anomaly having developed in the two decades after 1990 owing to above-normal

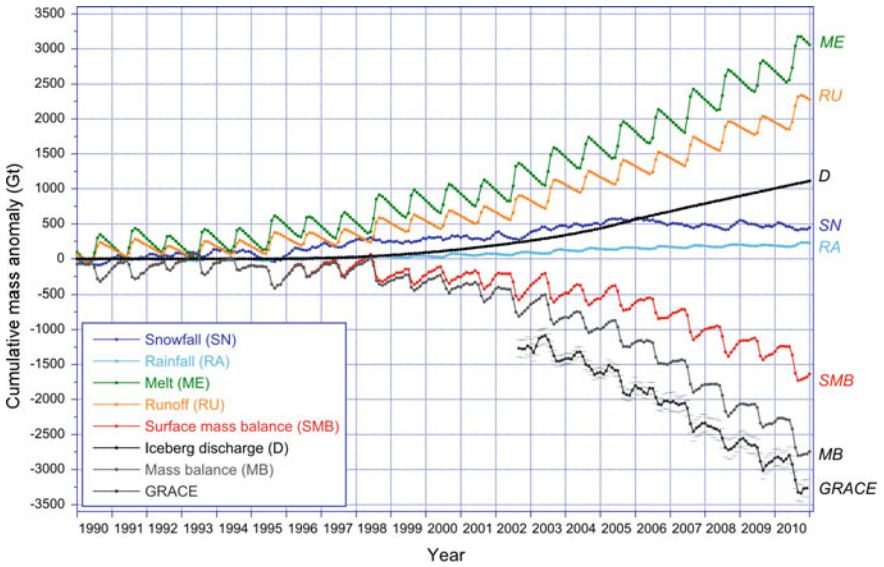

Fig. 7.16 Cumulative mass anomalies of GrIS mass balance (MB), surface mass balance (SMB) and liquid water balance components [35]. GRACE time series (data courtesy of I. Velicogna and J. Wahr) do not denote absolute values and have been vertically displaced for clarity

meltwater production. Increased rainfall added another 250 Gt to the liquid water mass anomaly. Only 2300 Gt ($\sim 70\%$) of this liquid water anomaly actually reached the ocean as runoff, the remainder is retained in the snowpack, mostly by refreezing and for a small part by capillary retention. Mass losses from the GrIS are further moderated by slightly enhanced snowfall (dark blue line), which added 500 Gt of mass. The total 1990–2010 surface mass balance (red line) anomaly is then ~ 1700 Gt, which, when added to the estimated mass loss through enhanced solid ice discharge (D, black line) results in a total negative mass anomaly of about 2800 Gt (dark grey line). The trend and seasonal cycle of the reconstructed mass loss compare very well with gravity measurements from space (GRACE, black line).

References

1. Cogley JG and 10 others (2011) Glossary of glacier mass balance and related terms. IHP-VII Technical Documents in Hydrology No. 86, IACS Contribution No. 2, UNESCO-IHP, Paris
2. Eisen O and 15 others (2008) Ground-based measurements of spatial and temporal variability of snow accumulation in East Antarctica. Revs Geophys 46:RG2001
3. Rotschky G, Holmlund P, Isaksson E, Mulvaney R, Oerter H, van den Broeke MR, Winther J-G (2007) A new surface accumulation map for western Dronning Maud Land, Antarctica, from interpolation of point measurements. J Glaciol 53(182):385–398
4. Lenaerts JTM, van den Broeke MR, van de Berg WJ, van Meijgaard E, Kuipers Munneke P (2012) A new, high-resolution surface mass balance map of Antarctica (1979–2010) based on regional atmospheric climate modeling. Geophys Res Lett 39(4):L04501

5. Helsen MM, van den Broeke MR, van de Wal RSW, van de Berg WJ, van Meijgaard E, Davis CH, Li Y, Goodwin I (2008) Elevation changes in Antarctica mainly determined by accumulation variability. Science 320(5883):1626–1629
6. Thomas R, Davis C, Frederick E, Krabill W, Li Y, Manizade S, Martin C (2008) A comparison of Greenland ice-sheet volume changes derived from altimetry measurements. J Glaciol 54(185):203–212
7. Pritchard HD, Arthern RJ, Vaughan DG, Edwards LA (2009) Extensive dynamic thinning on the margins of the Greenland and Antarctic ice sheets. Nature 461(7266):971–975
8. Ligtenberg SRM, Helsen MM, van den Broeke MR (2011) An improved semi-empirical model for the densification of Antarctic firn. The Cryosphere 5(4):809–819
9. Rignot E, Mouginot J, Scheuchl B (2011) Ice flow of the Antarctic Ice Sheet. Science 333(6048):1427–1430
10. Arthern RJ, Winebrenner DP, Vaughan DG (2006) Antarctic snow accumulation mapped using polarization of 4.3 cm wavelength microwave emission. J Geophys Res 111(D6):D06107
11. Bales RC, Guo Q, Shen D, McConnell JR, Du G, Burkhart JF, Spikes VB, Hanna E, Cappelen J (2009) Annual accumulation for Greenland updated using ice core data developed during 2000–2006 and analysis of daily coastal meteorological data. J Geophys Res 114:D06116
12. van de Berg WJ, van den Broeke MR, Reijmer CH, van Meijgaard E (2006) Reassessment of the Antarctic surface mass balance using calibrated output of a regional atmospheric climate model. J Geophys Res 111(D11):D11104
13. Ettema J, van den Broeke MR, van Meijgaard E, van de Berg WJ, Bamber JL, Box JE, Bales RC (2009) Higher surface mass balance of the Greenland ice sheet revealed by high-resolution climate modeling. Geophys Res Lett 36(12):L12501
14. Burgess EW, Forster RR, Box JE, Mosley-Thompson E, Bromwich DH, Bales RC, Smith LC (2010) A spatially calibrated model of annual accumulation rate on the Greenland Ice Sheet (1958–2007). J Geophys Res Earth Surf 115(F2):F02004
15. Joughin I, Das SB, King MA, Smith BE, Howat IM, Moon T (2008) Seasonal speedup along the western flank of the Greenland ice sheet. Science 320(5877):781–783
16. Bamber JL, Gomez-Dans JL, Griggs JA (2009) A new 1 km digital elevation model of the Antarctic derived from combined satellite radar and laser data—Part 1: data and methods. The Cryosphere 3(1):101–111
17. Rignot E, Bamber JL, van den Broeke MR, Davis C, Li Y, van de Berg WJ, van Meijgaard E (2008) Recent Antarctic ice mass loss from radar interferometry and regional climate modelling. Nat Geosci 1(2):106–110
18. Zemp M, Roer I, Kääb A, Hoelzle M, Paul F, Haeberli W (2008) Global glacier changes: facts and figures. United Nations Environmental Programme (UNEP) and World Glacier Monitoring Service
19. Zemp M, Nussbaumer SU, Gärtner-Roer I, Hoelzle M, Paul F, Haeberli W (eds) (2011) Glacier mass balance Bulletin No. 11 (2008–2009). ICSU (WDS)/IUGG (IACS)/UNEP/UNESCO/WMO, World Glacier Monitoring Service, Zurich, Switzerland
20. Hock R (2003) Temperature index melt modelling in mountain areas. J Hydrol 282:104–115
21. Giesen RH, Oerlemans J (2012) Calibration of a surface mass balance model for global-scale applications. The Cryosphere 6:1463–1481
22. Klok EJ, Oerlemans J (2002) Model study of the spatial distribution of the energy and mass balance of Morteratschgletscher, Switzerland. J Glaciol 48(163):505–518
23. Sedlar J, Hock R (2009) Testing longwave radiation parameterizations under clear and overcast skies at Storglaciären, Sweden. The Cryosphere 3:75–84
24. Pellicciotti F, Raschle T, Huerlimann T, Carenzo M, Burlando P (2011) Transmission of solar radiation through clouds on melting glaciers: a comparison of parameterizations and their impact on melt modelling. J Glaciol 57(202):367–381
25. Giesen RH, Oerlemans J (2010) Response of the ice cap Hardangerjøkulen in southern Norway to the 20th and 21st century climates. The Cryosphere 4:191–213
26. Cogley JG (2009) Geodetic and direct mass-balance measurements: comparison and joint analysis. Ann Glaciol 50(50):96–100

27. Arendt AA, Echelmeyer KA, Harrison WD, Lingle CS, Valentine VB (2002) Rapid wastage of Alaska glaciers and their contribution to rising sea level. Science 297(5580):382–386
28. Gardner AS, Moholdt G, Wouters B, Wolken GJ, Burgess DO, Sharp MJ, Cogley JG, Braun C, Labine C (2011) Sharply increased mass loss from glaciers and ice caps in the Canadian Arctic Archipelago. Nature 473:357–360
29. Rignot E, Rivera A, Casassa G (2003) Contribution of the Patagonia Icefields of South America to sea level rise. Science 302(5644):434–437
30. Jacob T, Wahr J, Pfeffer WT, Swenson S (2012) Recent contributions of glaciers and ice caps to sea level rise. Nature 482:514–518
31. Lenaerts JTM, van den Broeke MR, Scarchilli C, Agosta C (2012) Impact of model resolution on simulated wind, drifting snow and surface mass balance in Terre Adélie, East Antarctica. J Glaciol 58(211): 821–829
32. van den Broeke MR, Bamber J, Lenaerts J, Rignot E (2011) Ice sheets and sea level: thinking outside the box. Surv Geophys 32(4–5):495–505
33. Church JA, White NJ, Konikow LF, Domingues CM, Cogley JG, Rignot E, Gregory JM, van den Broeke MR, Monaghan AJ, Velicogna I (2011) Revisiting the Earth's sea-level and energy budgets from 1961 to 2008. Geophys Res Lett 38(18):L18601
34. Rignot E, Kanagaratnam P (2006) Changes in the velocity structure of the Greenland Ice Sheet. Science 311(5763):986–990
35. van den Broeke M, Bamber J, Ettema J, Rignot E, Schrama E, van de Berg WJ, van Meijgaard E, Velicogna I, Wouters B (2009) Partitioning recent Greenland mass loss. Science 326(5955):984–986